JOURNAL OF MATERIALS SCIENCE 29 (1994) 394–403

Photoelastic study of the durability of interfacial bonding of carbon fibre–epoxy resin composites

Z. R. XU*, K. H. G. ASHBEE‡
Materials Processing Center and Department of Materials Science and Engineering, The University of Tennessee, Knoxville, TN 37996-2200, USA

The physical techniques of polarizing microscopy, including the quantitative measurements of small optical retardations, have been used to investigate elastic fields adjacent to short carbon fibres in epoxy resin composites. The elastic fields associated with shear stress distribution along the fibre–matrix interface have been employed to monitor the initiation of interface debonding during hot (100 °C) water uptake. By examining the development of stress birefringence during resin swelling in the resin adjacent to individual fibres, the differences in the durability of interfacial bonding and the fibre failure modes for differently coated fibres have been obtained. The results show that the state of self-stress in model composites, comprising a single carbon fibre in a film of epoxy resin, can, by immersion in hot distilled water, be enhanced to such an extent that the axial tension in the fibre can be sufficient to initiate fibre fracture. The results also show that, for fibres that have been given certain proprietary surface treatments, the fibre fractures by different failure modes.

1. Introduction

Polymer-matrix composite materials have been gaining wide use in commercial, military and space applications because of their favourable performance characteristics. However, there is real concern because the mechanical properties of such materials are known to suffer when the material is exposed to moisture for long periods of time. Moisture-induced degradation of such composites can be the degradation of the fibre-matrix interface resulting in loss of load transfer [1] and interfacial bond strength [2], decrease of matrix modulus and strength [3], and loss of strength of the reinforced fibres due to leaching [4, 5] and stress corrosion.

Load transfer at the matrix–fibre interface is fundamental to the principle of fibre reinforcement. With weak interfacial bonding between fibre and matrix, the composite materials may behave like a bundle of fibres; with strong interfacial bonding, the composite materials may behave like a brittle monolithic solid. Owing to the sensitivity of the interface to water uptake, moisture-induced damage at the interface may be more profound than elsewhere. It is apparent that, in order to optimize the level of adhesion between fibre and matrix, the durability of interfacial bonding as well as the effects of surface treatments on the interfacial bonding, when the composite is exposed to moisture, must be known.

Unreinforced epoxy resin is optically isotropic. When reinforced with carbon fibres, epoxy resin adjacent to the fibres becomes optically anisotropic (birefregence) due to elastic stress (and possibly molecular orientation) arising from the net shrinkage of resin on to fibres that occurs during cooling from the resin curing temperature. If the resin is sufficiently transparent, the stress birefringence (photoelasticity) can be studied with polarized light. Since the phase difference of the two components of the polarized light resolved from a birefringent region of resin are determined by the stress field responsible for the birefringence, it is evident that, by studying the stress birefringence adjacent to fibres, it should be possible to deduce the nature of the stress field.

In the present work, the durability of interfacial bonding of carbon fibre–epoxy resin with different surface treatments has been investigated using photoelasticity. The results shown that, for fibres that have been given certain proprietary surface treatments, the durability of interfacial bonding has been improved and the fibre fractures by different failure modes.

2. Experimental procedure

2.1. Materials

Carbon fibres with five different proprietary surface treatments, designated A, B, C, D and E by Amoco Performance Products, have been studied. The fibres, of diameter about 8 μm, were chopped very carefully using a razor blade under a microscope into 1 mm lengths to be embedded in an epoxy resin, ERLX-1902.

* *Present address*: Department of Materials and Metallurgical Engineering, New Mexico Tech, Socorro, NM 87801, USA.
‡ *Present address*: 67 Abbey Foregate, Shrewsbury, SY2 6BG, UK.

0022–2461

A single carbon fibre is aligned axially in a glass mould for a rectangular coupon of length of 20 mm, width 5 mm and thickness 0.3 mm. The matrix material is poured into the cavity, and cured *in situ* in accordance with the manufacturer's recommended procedure: heating from room temperature to curing temperature 177.5 °C at a heating rate of 2.5 °C min^{-1}, then curing at 177.5 °C for 2 h and cooling from the curing temperature to room temperature at a cooling rate of 1.5 °C min^{-1}. A small furnace used for specimen fabrication was designed to accommodate degassing during curing and temperature control. The temperature of the curing cycle was controlled using a programmable temperature controller (Omega Series CN-2010). Also prepared in similar fashion were films of the same dimensions containing no fibres. These were used for measurements of overall resin dimensional changes.

All samples were immersed in distilled water at a temperature of 100 °C. The temperature of distilled water was automatically controlled by boiling it and cooling water prevented loss of distilled water by evaporation.

2.2. Measurement procedure

Stress-induced birefringence was observed and measured at room temperature using a Nikon transmission polarizing microscope (Optiphot-pol) with a Brice–Kohler compensator (0.05 λ) to measure small retardations, and a Sénarmont compensator (1 λ) to measure large retardations. The same Nikon microscopy was also used to measure dimensional changes during water immersion.

The stress-optical coefficient of epoxy resin after water uptake was obtained by measuring the retardation and an applied stress, the latter being measured by a load cell (Schaevitz MDTR-352L).

Since the birefringence pattern generated around a single fibre embedded in epoxy resin, and arising from the lack of correspondence between thermal contraction and moisture expansion, is of cylinder-like symmetry, a two-dimensional model can be employed for its analysis.

The tensile stress distribution around a single fibre embedded in a resin matrix under uniaxial loading was determined by Tyson and Davies [6] from a photoelastic investigation. It can be seen from their results that the tensile stress trajectories around the fibre end can be considered to have conic symmetry. According to our preliminary investigation, when a specimen is immersed in water, the stress birefringence disappears as we move in the direction perpendicular to the fibre axis, falling to zero within a distance of a few or ten fibre diameters from the fibre axis. Thus, by far the largest contribution to the observed stress birefringence is due to the stress near the interface. Furthermore, since the stress direction trajectories hereabouts change direction very slowly, say by 10° from the fibre axis out to where the birefringence disappears, the stress field can be approximated to one of circular symmetry. Consider one half of the cone of symmetry. If a coordinate system is chosen in which one axis is parallel to the conic line, this can be transformed into elliptic symmetry with $a/b = \cos\theta$. Since θ is very small, $a \simeq b$. This allows us to develop a photoelastic technique based on Poritsky's paper [7] to measure the shear stress and its distribution, and thus to monitor the progress of interfacial debonding.

Poritsky [7] showed that, for a long and uniform cylinder, the optical retardation R for a ray passing in a direction normal to the axis depends merely upon the principal stress in the axial direction, σ_{zz}, and the thickness, say, from a_1 to a_2, given by

$$R = 2\beta\int_{a_1}^{a_2} \sigma_{zz}\, dy$$

where β is the stress-optical coefficient, assumed to be a constant. In accordance with the definition of integrals, the integration can be obtained by adding a large number of units. Consider that the specimen consists of a large number of concentric rings and the total birefringence along a path of light is the sum of contributions of individual rings; then

$$R = 2\beta(\sigma_{zz_1}\Delta y_1 + \sigma_{zz_2}\Delta y_2 + \ldots + \sigma_{zz_n}\Delta y_n)$$

i.e.

$$R = 2\beta\sum_{i=1}^{n} \sigma_{zz_i}\Delta y_i$$

where n = number of rings traversed by a path of light, σ_{zz_i} = stress σ_{zz} in the ith ring and Δy_i = path length through the ith ring. If the number of rings is large enough, the stress in each ring can be regarded as constant. This calculation procedure of the internal stress was carried out by computer programming.

The interfacial shear stress, τ, can be monitored from the isochromatic (retardation) and isoclinic measurements as follows:

$$\tau = \frac{\sigma_{zz}}{2}\sin 2\zeta$$

where ζ is the isoclinic angle on inclination of σ_{zz} with respect to the fibre direction.

Using the assumption that elliptical symmetry, transferred from a system of conic symmetry, with its semi-axis ratio near to unity, can be treated as cylindrical symmetry, this technique can be employed to semi-quantitatively investigate the shear stress distribution at the interface, and hence can be used to monitor the interfacial debonding.

3. Results and discussion

3.1. Water uptake

In order to interpret effects arising from water immersion, it is important to know the dimensional changes undergone by resin during water immersion. Measurements of linear dimensional changes were made on epoxy films containing no fibres. Any dimensional changes of the mould during specimen fabrication were found to be too small to be detected. Hence the net dimensional changes of the epoxy resin after curing can be measured *in situ*. It turns out that the resin

linear shrinkage generated during fabrication is about 0.43% ((20.000 − 19.914)/20.000 = 0.43%).

Experimental measurements of changes in linear dimensions during water immersion for specimens containing no fibres (Fig. 1) demonstrate that the resin swelling is much greater than the resin shrinkage generated during fabrication. Since fibres can be assumed to be dimensionally stable relative to resins, it is evident that swelling of the epoxy matrix must be restrained by the fibres embedded in a composite. The overall result is that the volumetric swelling of the matrix produces tensile stress in a fibre and axial compressive stress in the matrix around the fibre, both of which are along the fibre direction as discussed below.

The change from shrinkage resulting from curing, to expansion resulting from water uptake, has been also detected by observing the changes in the directions of the optical axes of epoxy resin samples.

3.2. Effects of water uptake on stress-optical coefficient of epoxy resin

When using photoelastic analysis, it is necessary to know the stress-optical coefficient of the material studied. In order to investigate the moisture-induced degradation of composites by means of photoelasticity analysis, the effects of water uptake on the stress optical coefficient of matrix materials must be known. Measurements for the epoxy resin used in the present research have been made. Fig. 2 shows measurements of optical retardation versus tensile stress applied uniaxially on specimens of neat epoxy resin. The linear relationships between retardation and stress did not change during water immersion up to 300 h. The straight lines, which have almost the same slope, indicate that the stress-optical coefficient is constant, i.e. water uptake does not affect the stress-optical coefficients of the epoxy resins used in this experiment. By plotting the retardation (nm) against the applied stress (g mm^{-2}), the stress-optical coefficient can be found [8]. For the data shown in Fig. 2, the stress-optical coefficient is

$$\beta = 6.80 \times 10^{-8}\ \text{mm}^2\,\text{g}^{-1}$$

with standard deviation S given by

$$S = \left(\frac{\Sigma\beta^2 - \Sigma\bar{\beta}^2}{n-1}\right)^{1/2} = 2.34 \times 10^{-9}\ \text{mm}^2\,\text{g}^{-1}$$

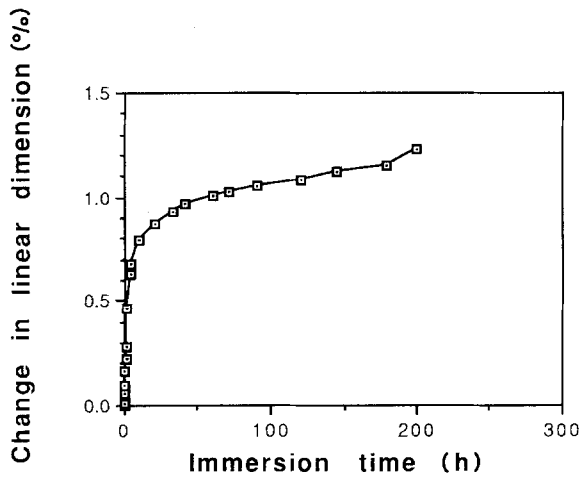

Figure 1 Linear dimensional changes of the net epoxy resin during immersion in distilled water at boiling temperature. Measurements were made at room temperature.

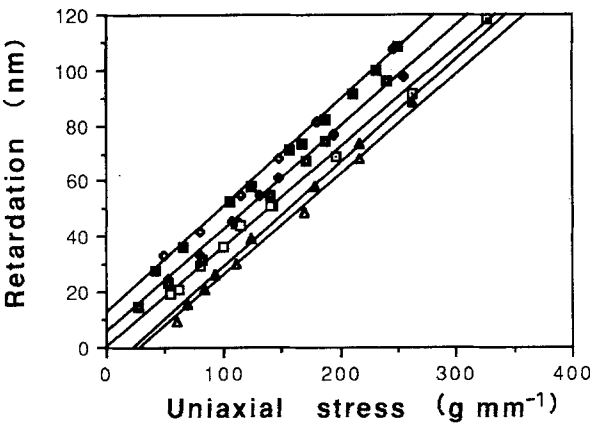

Figure 2 Retardation measured versus tensile stress applied uniaxially on a specimen of neat epoxy resin: (⊡) as received, (◆) 5 min, (■) 15 min, (◇) 35 min, (■) 95 min, (□) 150 min, (▲) 48 h, (△) dry + 12 h.

3.3. Durability of interfacial bonding

As pointed out above, epoxy resin undergoes shrinkages during curing and during cooling from the curing temperature to room temperature. Because the axial thermal expansion coefficient for most fibres is less than the thermal expansion coefficient of most matrix resins, a state of compression is generated in the resin adjacent to fibre ends. During water uptake, volumetric swelling occurs and this may be large enough to compensate for the compression, and eventually to leave the resin adjacent to fibre ends in a state of tension. Stress-induced birefringence measurements show the change of resin stress state from compression to tension as a reversal in the directions of fast and slow axes. Our experimental results show that the direction of the optical fast axis of the epoxy resin used in the present research is parallel to the direction of tension generated as mentioned above, while the direction of the optical slow axis is parallel to the direction of compression. The local distribution of stress-induced birefringence is also changed. Fig. 3a and b show the patterns of birefringence near fibre ends observed in a specimen before water immersion. Extinction along the fibre direction when viewed at 0° to the polarizer axes follows from the condition for isoclinic fringe formation, where the principal axis of either σ_1 or σ_2 coincides with the axis of polarization of either the analyser or the polarizer. Comparing with the original patterns, Fig. 3c shows that, for the same fibre, the patterns of birefringence change in extent as well as in nature after water uptake. In order to interpret these changes, retardation measurements have been made (Fig. 4). The retardation increases as the amount of swelling increases.

Fig. 5 shows retardation measurements made near the fibre end at points along a radial direction from a fibre totally embedded in epoxy resin and immersed

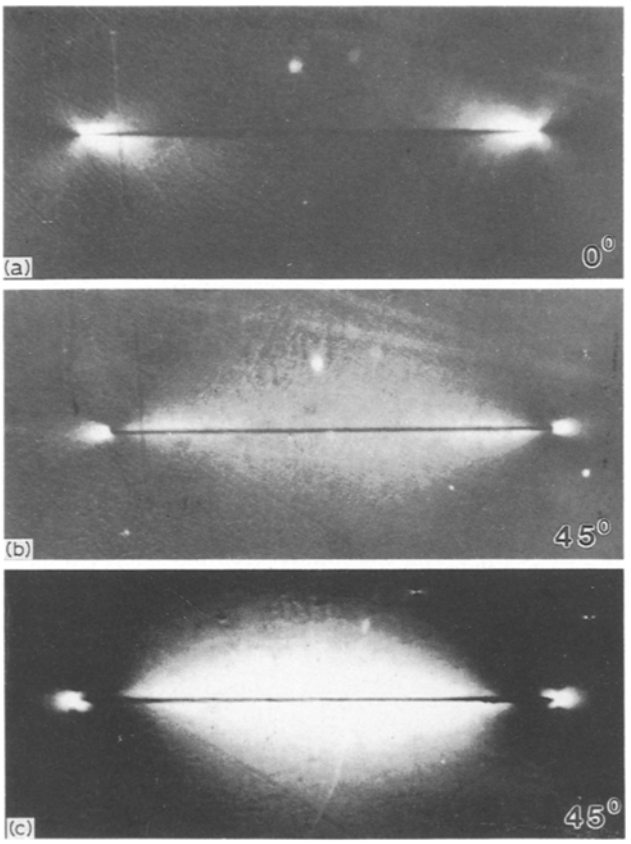

Figure 3 Patterns of stress-induced birefringence around a single fibre totally embedded in a film of epoxy resin. Before water immersion: viewed at (a) 0° to the polarizer axes and (b) at 45° to the axes; and after water immersion (c) at 45° to the axes.

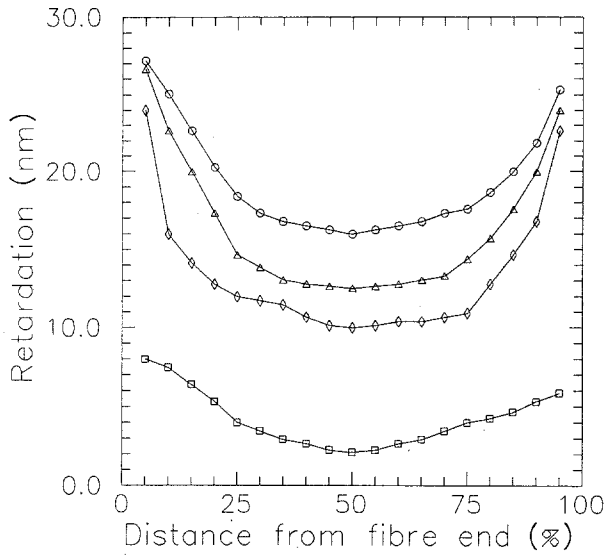

Figure 4 Increases of retardation as immersion time increases: (◇) original, (□) 20 min, (△) 4 h, (○) 10 5 h.

in boiling water. Using the procedure described above, the magnitude of the stress in the epoxy resin acting parallel to the fibre axis can be obtained, and is also shown in Fig. 5. It is seen that the axial stress is concentrated at the fibre–matrix interface. As discussed above, the retardation measured using the model is the sum of contributions from individual

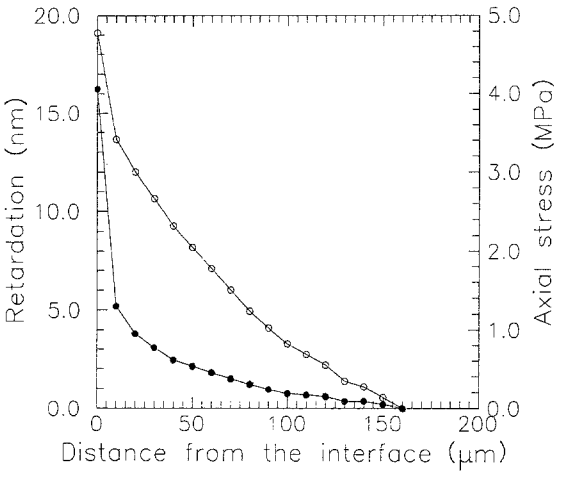

Figure 5 (○) Typical retardation measurements made near fibre ends at points along a radial direction from a fibre totally embedded in epoxy resin and immersed in boiling water, and (●) magnitude of associated stress in the epoxy resin acting parallel to the fibre axis.

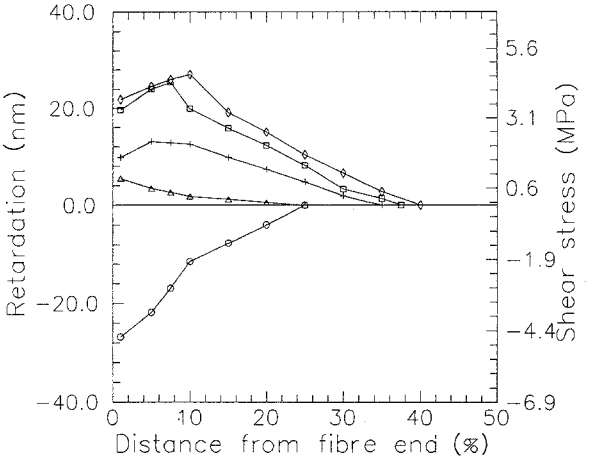

Figure 6 Fibre B: optical retardation changes close to the interface during boiling water uptake. (○) Original, (△) 20 min, (+) 1 h, (□) 10.5 h. (◇) 22.5 h.

rings. Since most of the stress is concentrated near the interface, it is here that the stress-induced birefringence makes its most important contribution to the measured retardation, i.e. retardation measurements made close to the interface are more important than those made further away.

So, to investigate interfacial bond behaviour during water uptake, the distribution of interfacial shear stress close to the interface between fibre and matrix is of most significance. Since the overall retardation measured is the sum of contributions from elastic and plastic deformation (here the plastic portion has been neglected), and since a cylindrical model is assumed, the shear stresses listed are at best only semi-quantitative. Fig. 6 shows the shear stress distribution close to the interface for fibre B. Initially, the stress in the resin adjacent to the fibre is compressive, giving rise to a direction of shear stress towards the fibre end identified as negative. After water uptake, the direction of the shear stress changes and the directions of optical fast and slow axes reverse. With increasing time of water uptake, the position of maximum shear stress

migrates towards the fibre centre, as revealed in Fig. 6. This can be interpreted by considering the mechanism of load transfer. With perfect interfacial bonding, the maximum shear stress occurs at the end of the fibre (a more sophisticated model [9] shows that the position of maximum shear stress is very close to but not at the end of the fibre), and may be large enough to exceed the strength of interfacial bonding. If so, debonding occurs. The position of highest shear stress is then no longer at the fibre end, but has moved towards the centre of the fibre.

If the time for the position carrying maximum shear stress to migrate, say, by a distance of one fibre diameter towards the centre of the fibre is taken as the criterion for the onset of debonding, the debonding times for different fibre surface treatments can be compared. Fig. 7 shows shear stress distributions for a specimen containing a length of fibre C. The interfacial debonding, as defined here, is established after 20 min of water uptake. Fig. 8 shows the time needed for specimens containing each of fibres A, B, C, D and E to debond. This bar chart was constructed using data from three specimens for each fibre and the times shown are the average values. It is seen that fibre B offers the longest durability and fibre C offers the least durability against uptake of water of 100 °C.

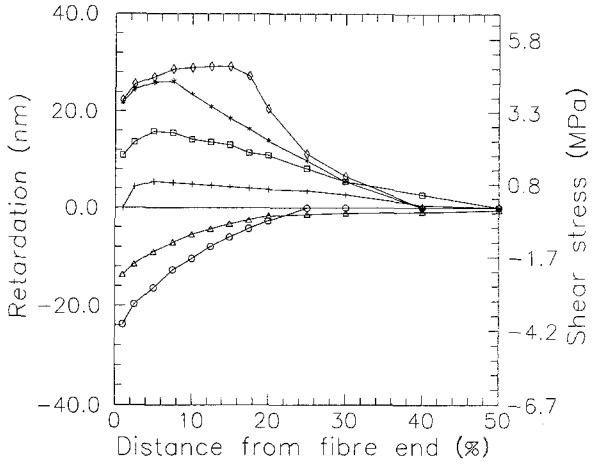

Figure 7 Fibre C: optical retardation changes close to the interface during boiling water uptake. (○) Original, (△) 10 min, (+) 20 min, (□) 1 h, (∗) 4 h, (◇) 10.5 h.

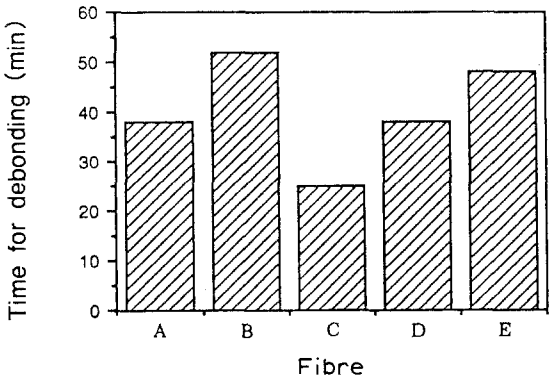

Figure 8 Immersion time needed for specimens containing each of fibres A, B, C, D and E to debond.

3.4. Fracture of fibres

Viewed with monochromatic light between crossed polarizing filters and oriented at 45° to the fast and slow directions, the entire specimen exhibited a changing sequence of birefringence patterns during the water immersion test. Once the fibre begins to fracture, a characteristic birefringence pattern develops adjacent to the broken fibre ends, since the stress state changes significantly. Fig. 9 shows the changing pattern of stress-induced resin birefringence for fibre B during a water immersion test. After immersion for 10.5 h the birefringence (Fig. 9b) is very different from the initial pattern (Fig. 9a). Not only has compensation occurred for the "compressive" birefringence; a net "tensile" birefringence has taken its place. As water uptake continues, more volumetric swelling of the matrix occurs, the axial tensile stress in the fibre increases [10], and eventually becomes large enough to fracture the fibre (Fig. 9c). A further increase in immersion time causes the region of birefringence at the fibre break to enlarge (Fig. 9d).

A very different sequence of birefringence patterns was observed for fibre C (Fig. 10). After 151 h immer-

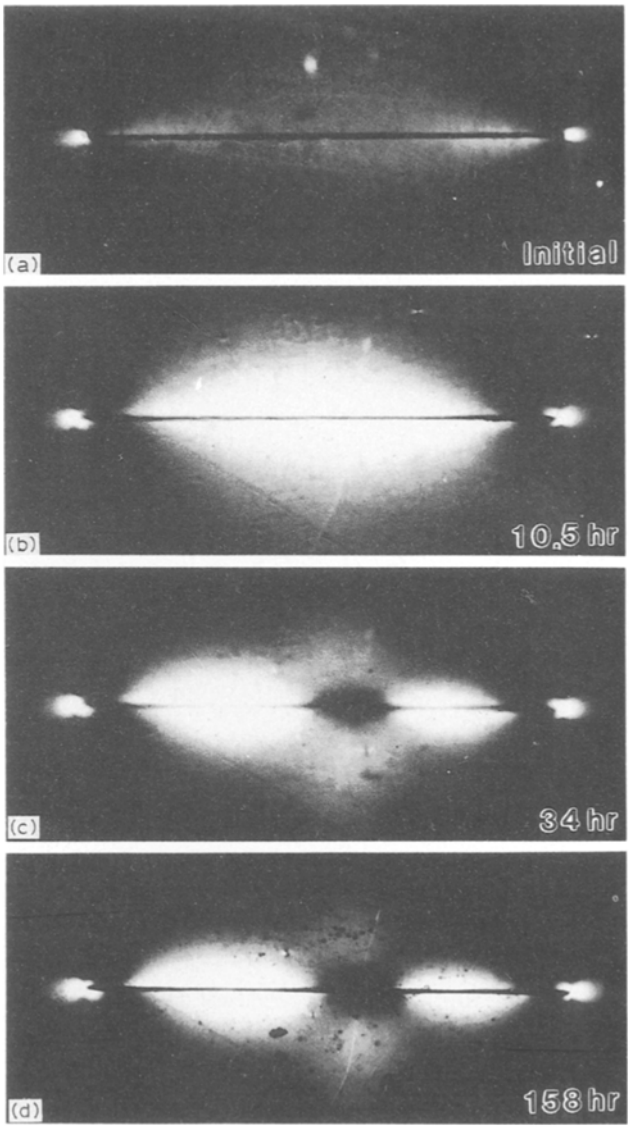

Figure 9(a–d) Sequence pattern of stress-induced birefringence of fibre B during water immersion, viewed at 45° to the polarizer axes.

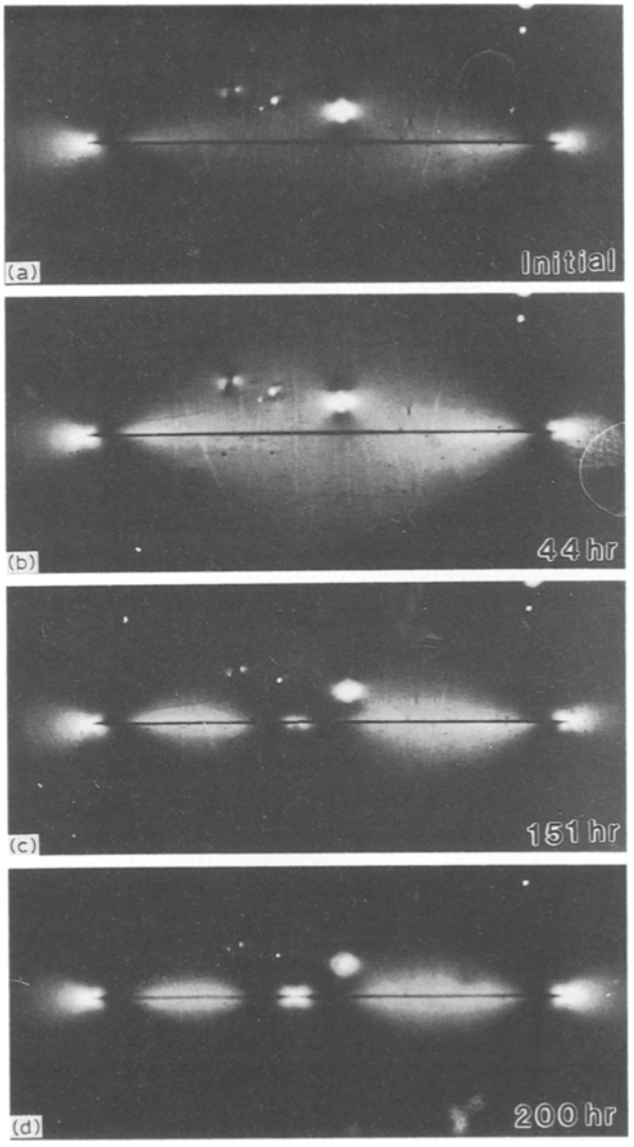

Figure 10(a–d) Sequence pattern of stress-induced birefringence of fibre C during water immersion, viewed at 45° to the polarizer axes.

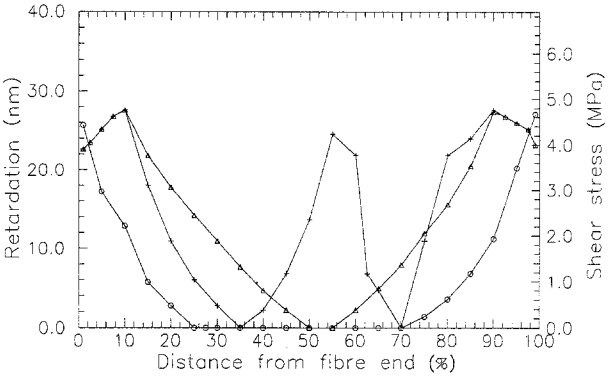

Figure 11 Fibre B: optical retardation measured through the resin adjacent to the interface and the corresponding interfacial shear stress, plotted as a function of both fibre length and immersion time. (○) Original, (△) 22.5 h, (+) 34 h.

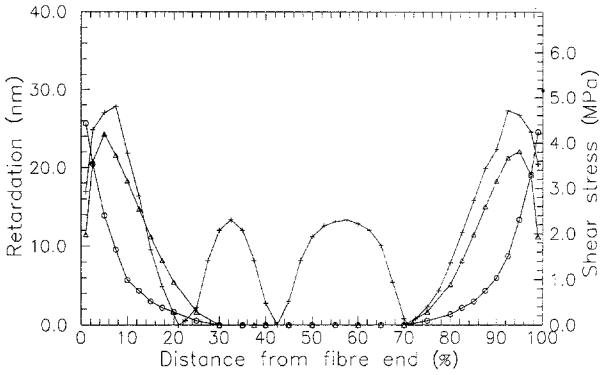

Figure 12 Fibre C: optical retardation measured through the resin adjacent to the interface and the corresponding interfacial shear stress, plotted as a function of both fibre length and immersion time. (○) original, (△) 103 h, (+) 151 h.

sion the fibre began to fracture, evidence for which is the change of birefringence pattern in Fig. 10c. The difference in the birefringence pattern associated with fibre fracture in Fig. 9c and 10c suggests a failure mode different from that for specimen B. From a careful examination of these patterns, one common feature and two main differences between the two patterns can be seen. Common in these two fibre failure modes is the fact that the fibres have fractured into two approximately equal lengths, i.e. fracture occurs at the fibre centre where the axial tensile stress is a maximum [11]. The axial tension generated along the fibre during water uptake by load transfer via interfacial shear stress can be large enough to fracture the fibre. Of the differences, one is the time required for fibre fracture. Fracture occurred after 10.5 h immersion for fibre B and after 151 h for fibre C.

The second difference concerns the patterns of stress-induced birefringence. When viewed at 45° to the polarizer axes, the pattern of birefringence near a fibre fracture is one of extinction (black contrast) for fibre B (Fig. 9c), and one of non-extinction (white contrast) for fibre C (Fig. 10c). This difference reveals a characteristic difference in fracture mode.

In order to explain the difference, the respective optical retardations have been carefully measured. Fig. 11 shows optical retardation data measured adjacent to the interface and the associated shear stress, plotted as a function of fibre length and immersion time. After fibre B fractures, the shear stress near the fracture is still very large. For fibre C, the retardation measurements (Fig. 12) show that the shear stress near the fibre fracture is relieved by the fracture process, i.e. debonding has occurred in association with the fibre fracture. Fig. 13a shows a schematic diagram for the fracture mode observed in fibre B, which is a disc-shaped or penny-shaped crack oriented perpendicular to the fibre and extending into matrix material. The stress state at fracture is also sketched in Fig. 13a. When the directions of principal stress are coincident with the polarization direction of the polarizer and analyser, extinction occurs. For the stress state in Fig. 13a there are some principal stresses having a 45° direction relative to the fibre axis (note that stresses σ_1 and σ_2 in Fig. 13a are not principal stresses), near the fibre fracture since there are large shear stresses. When the fibre axis is at 45° to the axes of the polarizer and analyser, extinction is observed. When the fibre

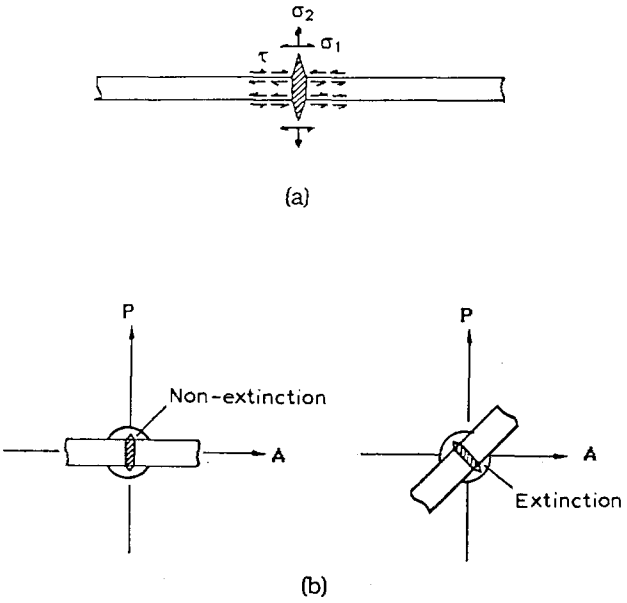

Figure 13 (a) Schematic diagram of failure mode observed in fibre B; (b) stress birefringence observed with fibre axis at 0 and 45° to the polarizer (P) and analyser (A) axes.

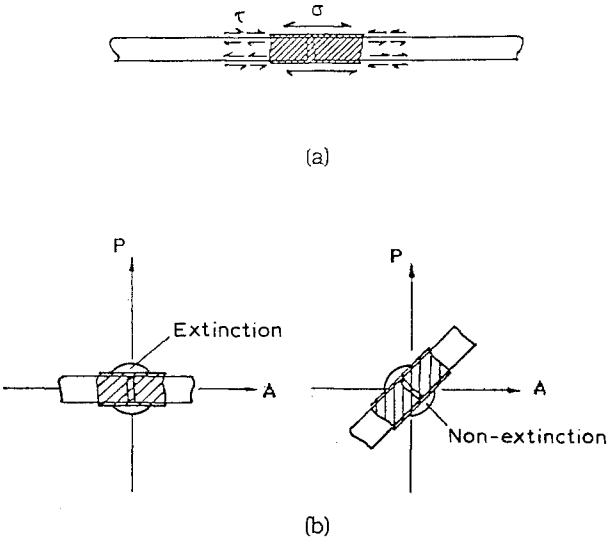

Figure 15 (a) Schematic diagram of failure mode observed in fibre C; (b) stress birefringence observed with fibre axis at 0 and 45° to the polarizer (P) and analyser (A) axes.

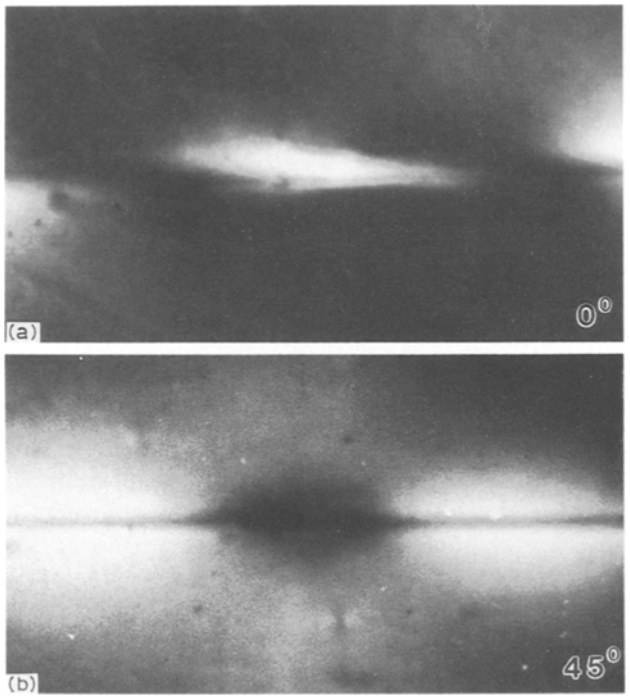

Figure 14 Patterns of stress-induced birefringence near the fracture of fibre B, viewed at (a) 0° and (b) 45° to the polarizer axes.

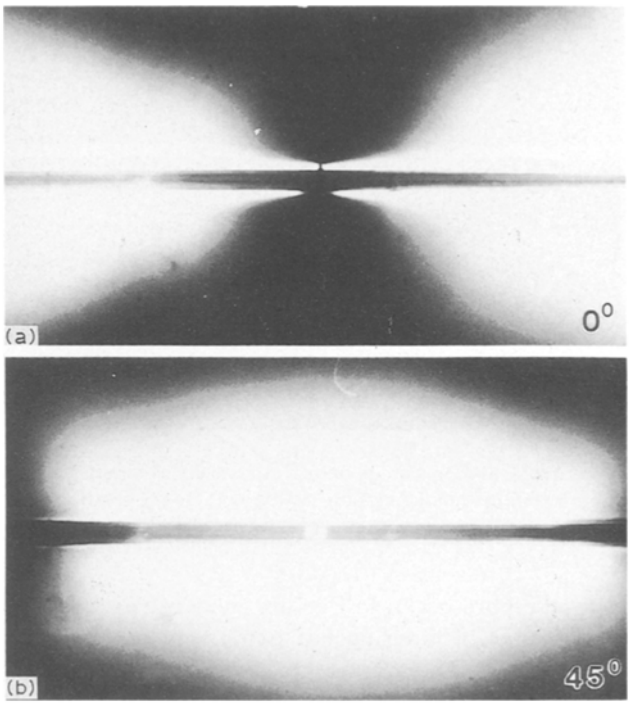

Figure 16 Patterns of stress-induced birefringence near the fracture of fibre C, viewed at (a) 0° and (b) 45° to the polarizer axes.

axes is at 0° to the axes of the polarizers, extinction is not observed, (see Fig. 13b and Fig. 14).

Using the same procedure, the stress state near the fibre fracture for fibre C can be identified and is sketched in Fig. 15a. Since there is no shear stress near the fibre fracture, the directions of principal stress must be parallel to and perpendicular to the direction of the fibre axis. When the fibre axis is coincident with the polarization direction of either the polarizer or the analyser, the condition for extinction is satisfied. Fig. 15b shows the conditions for extinction and non-extinction. This analysis is consistent with experimental observation. Fig. 16 shows what has been seen for fibre C. When viewed at 0° to the axes of the polarizer and the analyser, the pattern appears dark, whereas when viewed at 45° to the axes the pattern appears bright. As the water immersion test continues, and more stress is generated, the crack propagates as shown in Figs 17 and 18.

Fig. 19 shows SEM confirmation of the fracture of fibre B; a "penny-shaped" crack has propagated from the fibre into the epoxy matrix. Similar crack propagation from single fibres has been observed for fibres A, D and E (Fig. 20).

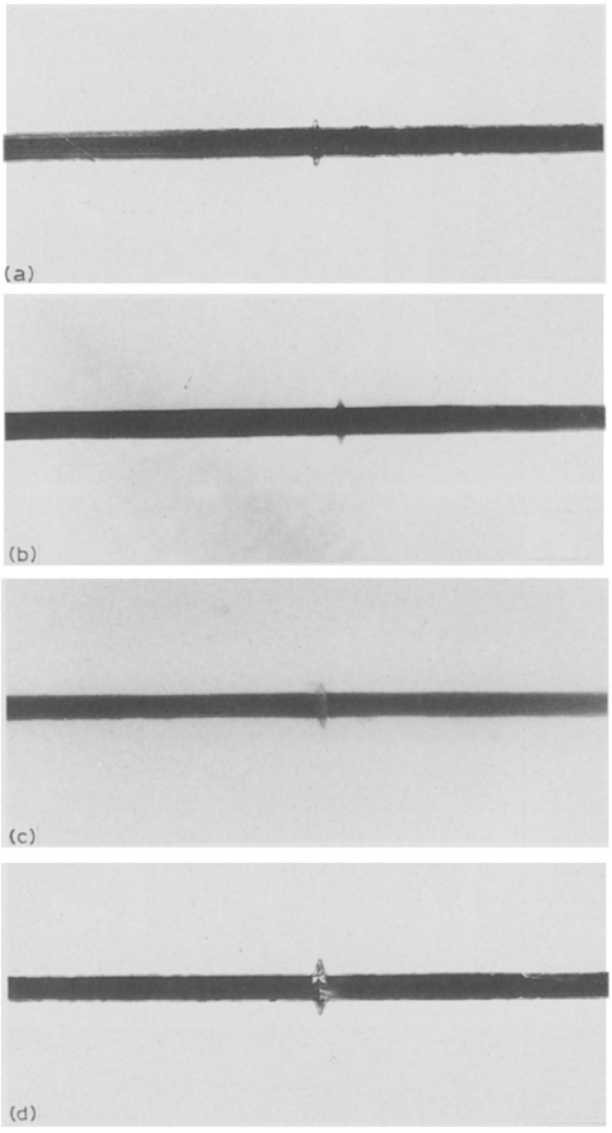

Figure 17 Sequence of fracture of a single carbon fibre B in epoxy resin after immersion in water at boiling temperature: (a) 34 h, (b) 158 h, (c) 525 h, (d) 1500 h.

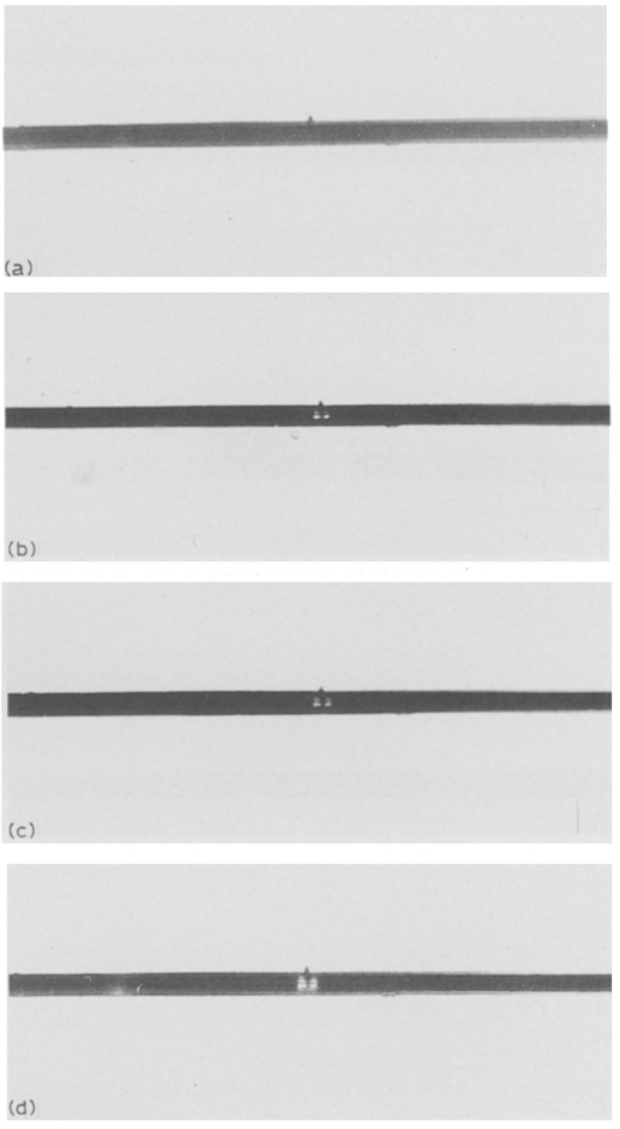

Figure 18 Sequence of fracture of a single carbon fibre C in epoxy resin after immersion in water at boiling temperature: (a) 151 h, (b) 200 h, (c) 415 h, (d) 1080 h.

3.5. Fibre pull-out length

Fig. 21 shows two typical fracture surfaces of composite specimens pulled in tension parallel to the fibre direction after 14 days immersion in boiling distilled water. Fig. 22 shows the distributions of fibre pull-out lengths seen in Fig. 21. The differences in pull-out lengths of fibres reflect differences in strength and differences in the longevity of interfacial bonding. The stronger the interfacial bonding, the shorter the pull-out length; the more resistant the interfacial bonding is to attack by the aqueous environment, the shorter the pull-out length. This is controlled by the different responses of the surface treatments to the aqueous environment.

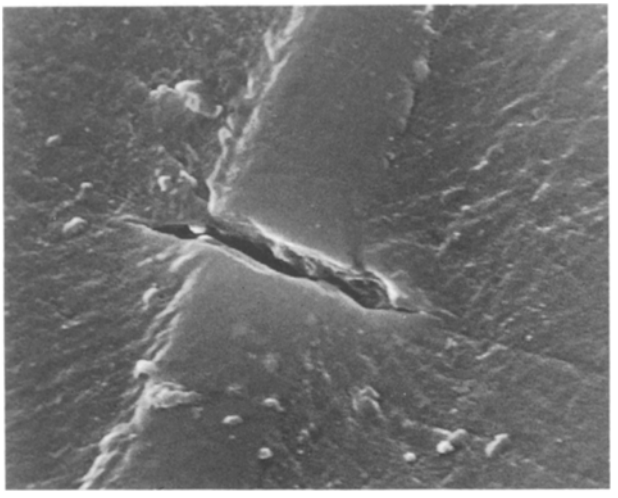

Figure 19 SEM observation of fibre fracture (fibre B) in matrix self-stressed by water uptake.

4. Concluding remarks

The advent of improved fibre surface preparations for carbon fibre is well illustrated by these experiments. The durability of load transfer between matrix resin and fibre has been enhanced to such an extent that swelling deformations large enough to fracture the fibre can be realized. Any reduction in the ability of a fibre–matrix interface to support shear stress will diminish the rate of increase of fibre axial stress with

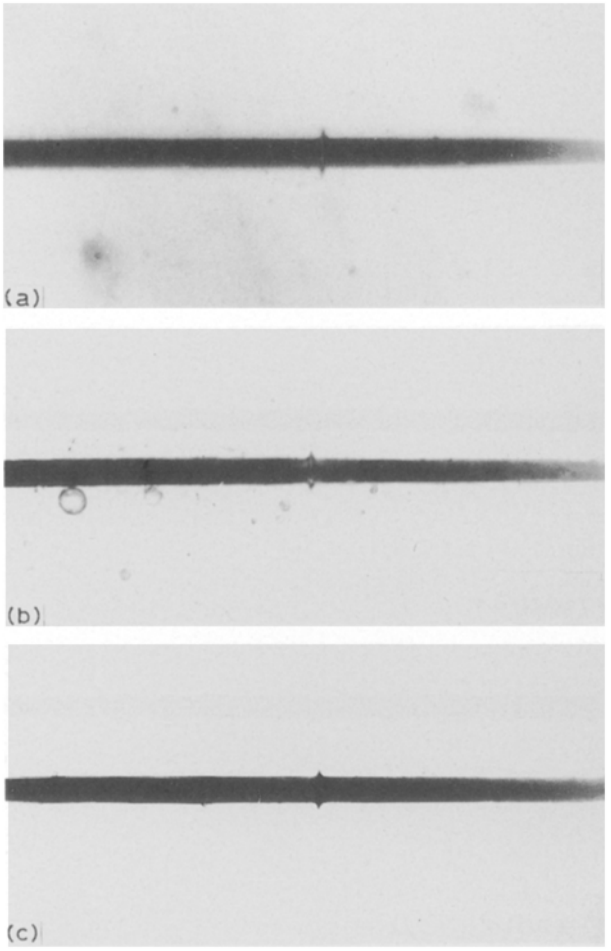

Figure 20 Similar crack propagation from single fibres for (a) fibre A, (b) fibre (D) and (c) fibre E.

distance from the fibre end. For the extreme case of an interface incapable of supporting any shear stress, there can be no build-up of axial fibre stress. The patterns of resin stress birefringence shown in Figs 9 and 10 indicate that the fibre has fractured into two approximately equal lengths; that is, fracture of fibre occurs at the fibre centre where the axial tensile stress is in a maximum. The longer the interfacial bonds survive during water immersion, the higher the build-up of axial fibre stress and hence, the sooner the occurrence of fibre fracture. From this point of view, the interfacial bonds of fibre B (whose fracture occurred after 10.5 h immersion) may have survived longer than those of fibre C (fracture after 151 h immersion). These conclusions are consistent with the experimental results for the immersion time required for different fibres to debond interfacially. Fig. 23 shows the times required for the occurrences of debonding and fracture for all five fibres. The longer the interfacial bonds survive during water immersion, the shorter the time before fibre fracture occurs. The same conclusion was also reached from the SEM observations in Fig. 21 of the fracture surfaces of tensile test specimens.

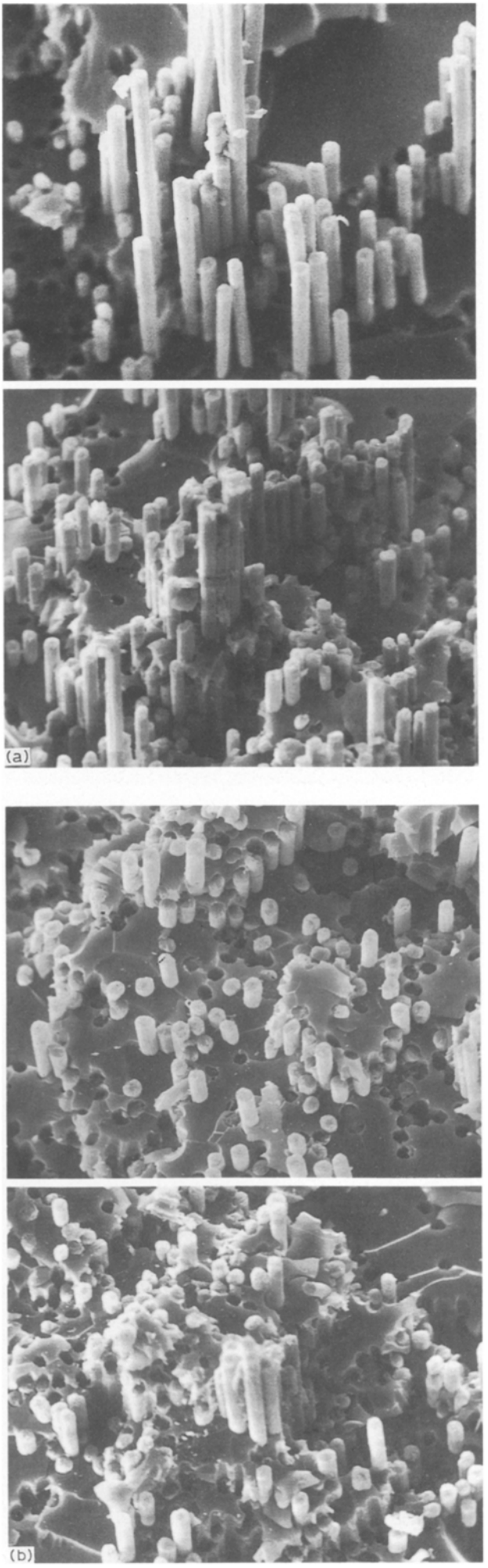

Figure 21 SEM observation of typical fracture surface of specimens after 14 days immersion in distilled water at boiling temperature: (a) specimen containing a bundle of fibre B, (b) specimen containing a bundle of fibre C.

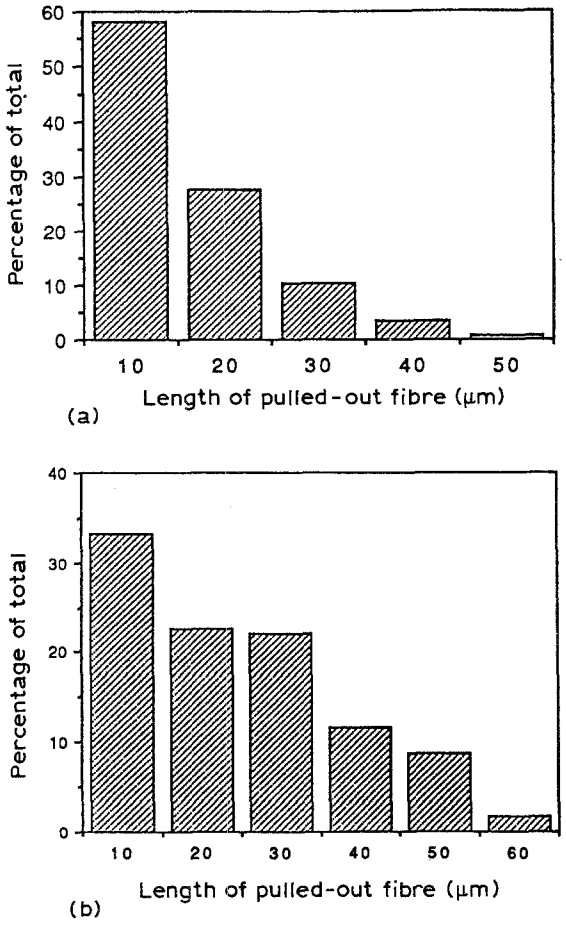

Figure 22 Distribution of pulled-out lengths of fibre under the same conditions as Fig. 21: (a) specimens containing a bundle of fibre B, (b) specimens containing a bundle of fibre C.

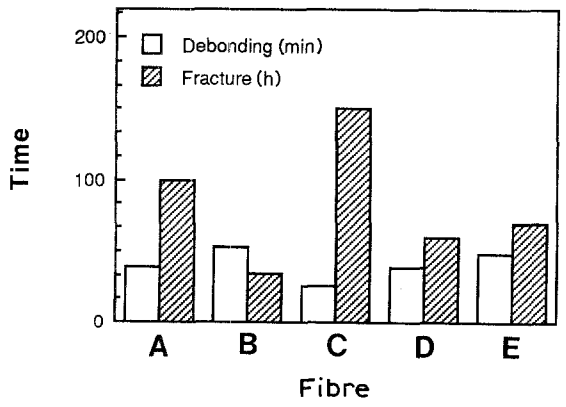

Figure 23 Times required for the occurrence of debonding and fracture for all the five fibres.

As discussed above, the effectiveness of reinforcement depends in a very fundamental way upon the stress transfer between fibre and matrix. Stress transfer, however, is limited by the strength of the "interfacial region", i.e. the material within the matrix and adjacent to the surface of the fibre. This material is very much affected by the different surface treatments. The mechanical behaviour of the interfacial region also controls the stress distribution that leads to fibre fracture. In the wholly elastic case, the maximum interfacial shear stress occurs at the fibre ends, and here we include fibre breaks. If the high shear stress concentration exceeds the interfacial region strength, there is local debonding of matrix from the fibre for some distance from the fibre break. This debonding displaces the shear stress concentration towards the centres of the remaining fibre lengths. The matrix adjacent to the fibre at the fracture location is suddenly stressed so as to carry the tension previously carried by the fibre. If the tensile strength of the matrix is exceeded, the fibre break-up propagates into the matrix to form a disc-shaped crack normal to the fibre axis.

Two distinct types of fibre failure behaviour have been observed. The energy released during fracture of these specimens accounts for the fracture surface energies of the fibre and matrix materials, and of interfacial cracks. If there exists sufficient bonding between matrix and fibre, the extent to which a disc-shaped or penny-shaped crack propagates into the resin depends upon the ability of the matrix to absorb energy at the ever-increasing circumference of the crack. On the other hand, debonding at the interface between fibre and matrix can relieve the stress concentration induced by fibre fracture and can prevent propagation into the matrix. The energy released and the energy absorbed, and the conditions for these two cases occurring, have been discussed by Mullin and Mazzio [12].

Acknowledgement

The authors gratefully acknowledge the gift of carbon fibre arranged by I. M. Kowalski of Amoco Performance Products, Inc.

References

1. R. C. WYATT and K. H. G. ASHBEE, *Fibre. Sci. Tech.* **2** (1969) 29.
2. B. MILLER and U. GAUR, in "Proceedings of 5th International Joint Military/Government Industry Symposium on Structural Adhesive Bonding", US Armament Research Development and Engineering Centre, Picatinny, Arsenal, Dover, NJ, 3–5 November, 1987, p. 280.
3. C. E. BROWNING, G. E. HUSMAN and J. M. WHITNEY, ASTM STP 617 (American Society for Testing and Materials, Philadelphia, 1977) p. 481.
4. L. HOLLAND, "The Properties of Glass Surface" (Chapman & Hall, London, 1966) p. 182.
5. S. M. WIEDERHORN and L. H. BOLZ, *J. Amer. Ceram. Soc.* **53** (1970) 543.
6. W. R. TYSON and G. I. DAVIS, *Br. J. Appl. Phys.* **16** (1965) 199.
7. H. PORITSKY, *Physics* **5** (1934) 406.
8. A. KUSKE and G. ROBERTSON, "Photoelastic Stress Analysis" (Wiley, London, 1974) p. 82.
9. J. M. WHITNEY and L. T. DRZAL, ASTM STP 937 (American Society for Testing and Materials, Philadelphia, 1987) p. 179.
10. Z. R. XU and K. H. G. ASHBEE, *J. Compos. Mater.* **25** (1991) 760.
11. H. L. COX, *J. Appl. Phys.* **3** (1952) 72.
12. J. MULLIN and J. M. MAZZIO, "Basic Failure Mechanisms in Advanced Composites", Final Report to NASA, Contract No. NASw-2093. (National Technical Information Service, Springfield, va 22151).

Received 30 July 1992
and accepted 23 February 1993